BIOCHEMISTRY
including biophysical chemistry & molecular biology

Article

pubs.acs.org/biochemistry

The Structure, Dynamics, and Binding of the LA45 Module Pair of the Low-Density Lipoprotein Receptor Suggest an Important Role for LA4 in Ligand Release

Miklos Guttman and Elizabeth A. Komives*

Department of Chemistry and Biochemistry, University of California at San Diego, 9500 Gilman Drive, La Jolla, California 92093-0378, United States

Supporting Information

ABSTRACT: The low-density lipoprotein receptor (LDLR), the primary receptor for cholesterol uptake, binds ligands through its seven LDL-A modules (LAs). We present nuclear magnetic resonance (NMR) and ligand binding measurements on the fourth and fifth modules of the LDLR (LA45), the modules critical for ApoE binding, at physiological pH. Unlike LA5 and all other modules in LDLR, LA4 has a very weak calcium affinity, which probably plays a critical role in endosomal ligand release. The NMR solution structure of each module in the LA45 pair only showed minor differences compared to the analogous domains in previously determined crystal structures. The 12-residue linker connecting the modules, though slightly structured through an interaction with LA4, is highly flexible. Although no intermodule nuclear Overhauser effects were detected, chemical shift perturbations and backbone dynamics suggest cross talk between the two modules. The ligand affinity of both modules is enhanced when the two are linked. LA4 is more flexible than LA5 and remains so even in the module pair, which likely is related to its weaker calcium binding affinity.

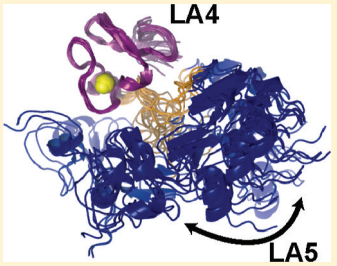

The low-density lipoprotein receptor family is critical for the uptake of cholesterol-containing lipoprotein particles. The best-characterized of these is the low-density lipoprotein receptor (LDLR), which contains seven LDL-A (LA) modules that mediate ligand interactions (Figure 1).[1] Once ligand binding occurs, the receptor−ligand complex is endocytosed and ligand is released. Upon endocytosis, the lower pH within the endosome triggers an intramolecular interaction between the LA modules and the β-propeller domain causing ligand release by way of displacement.[2] However, the significantly lower pH and calcium ion concentration within the endosome have also been suggested to promote ligand release independent of this displacement mechanism.[3]

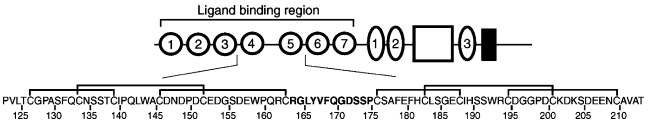

Figure 1. Schematic diagram of the LDL receptor with ligand binding modules (circles), EGF-like repeats (ovals), the β-propeller domain (open rectangle), and the transmembrane domain (filled rectangle). The sequence of LA45 with the linker (bold) is also shown with residues numbered according to the mature protein sequence with bold lines indicating disulfide bonds.

The structures of several LA modules from LDLR and related receptors have been determined by both X-ray crystallography[2,4−6] and nuclear magnetic resonance (NMR).[7−9] All of these share a conserved disulfide pattern and a calcium binding site,[10,11] resulting in a common fold. The specificity of ligand binding is thought to be determined mainly through exposed nonconserved residues.[1] Each module is linked to its neighbor by a four- or five-residue linker, except for the fourth (LA4) and fifth (LA5) LDLR modules, which have a 12-residue linker. It is believed that LA modules behave in a manner independent of their neighbors like beads on a string.[12−15]

The LA modules in LDLR have a high affinity for several physiological ligands, including apolipoprotein E (ApoE)-containing β-VLDL particles.[16] Ligand binding assays with recombinant LDLR from which single modules were deleted showed that LA5, and to a lesser extent LA4, were the key modules for mediating β-VLDL binding.[17] The same study showed that deletion of the extra long linker between LA4 and LA5 can affect the binding of certain ligands. The LA45 module pair was later shown to be the minimal unit of LDLR to bind β-VLDL-mimicking ApoE·dimyristoylphosphatidylcholine (DMPC) particles in vitro.[18] The order of these critical modules is also important as swapping the position of LA5 in LDLR also impaired ligand binding.[19]

The structures of LA5 at low pH, LA34 complexed with domain 3 of the receptor-associated protein (RAP), and the entire LDLR at endosomal pH have been determined,[2,4,6] but the structure and behavior of LA45 at physiological pH, presumably the form that binds ApoE, remain elusive.[20] Here we report the NMR structure, calcium binding properties, and

Received: September 16, 2011
Revised: November 16, 2011
Published: November 17, 2011

backbone dynamics of the LA45 module pair revealing some unique properties of this critical module pair.

METHODS

Protein Expression. LDLR LA fragments were cloned, expressed, purified, and refolded as described previously.[21] Constructs containing LA4 were further purified by reverse phase HPLC [DELTA-PAK column, 300 mm × 19 mm (inside diameter), 15 μm, 300A C18 (Waters)] in 10 mM NH_4OAc (pH 5.5) containing 5 mM $CaCl_2$ with a linear acetonitrile gradient (10 to 50%) at a rate of 10 mL/min. For calcium binding studies, LA constructs were repurified with a 10 to 50% acetonitrile gradient using 0.1% trifluoroacetic acid (TFA) to remove calcium ions. Proteins were lyophilized and stored at −20 °C. Masses of the final proteins were confirmed by MALDI-TOF (Voyager DESTR, Applied Biosystems) mass spectrometry. Size exclusion chromatography indicated that the refolded proteins were monomeric.

All of the LDLR ligands were prepared as ubiquitin fusions because this aided in the solubility of ApoE(130−149). A ubiquitin (Ub) fusion vector was generated by cloning the DNA sequence for ubiquitin into the NcoI and BamHI sites of vector pHis8.[22] RAPD3 (residues 252−357) was introduced between the BamHI and NotI sites to generate a His8-Ub-RAPD3 construct. The same strategy was used to generate His8-Ub-ApoE(130−149). A stop codon was inserted at the C-terminal end of Ub to generate a His8-Ub construct that was used to prepare free Ub as a negative control ligand. Proteins were produced in BL21-DE3 cells, grown in LB to an OD_{600} of 0.5, and induced with 0.1 mM isopropyl β-D-thiogalactopyranoside (IPTG) for 4 h at 37 °C. Cells were harvested, resuspended in TBS [50 mM Tris (pH 8.0) and 500 mM NaCl], and lysed by sonication, and the protein was purified by Ni-NTA (Qiagen) and size exclusion (Sephadex 75, GE Healthcare) in 20 mM Hepes (pH 7.45), 150 mM NaCl, 10 mM $CaCl_2$, and 0.02% azide. For Ub-ApoE(130−149), an additional cation exchange step (MonoS, GE Healthcare) using a gradient from 0 to 750 mM NaCl was necessary prior to size exclusion.

Isothermal Titration Calorimetry (ITC). Calcium binding titrations were performed on a MicroCal VP-ITC calorimeter at 35 °C. Dried protein was resuspended (250 μM) in Chelex (Bio-Rad)-treated buffer [20 mM Hepes (pH 7.4), 150 mM NaCl, and 0.02% azide]. Each protein was titrated with 2.5 mM $CaCl_2$ in the same buffer. LA4 titration was repeated using 5 mM $CaCl_2$, at pH 7.4 and also at pH 5.2. Data were fit in Origin 6.0 (OriginLab).

NMR. NMR experiments were conducted at 33 °C on a 600 MHz Bruker AvanceIII spectrometer equipped with a cryoprobe. Dried proteins were dissolved to a final concentration of 0.7−1 mM in 20 mM d_{18}-Hepes (Cambridge Isotope Laboratories) (pH 7.45), 150 mM NaCl, 5 mM $CaCl_2$, 10% D_2O, and 0.02% sodium azide. Backbone resonances were assigned via CBCA(CO)NH,[23] CBCANH,[24] and HNCO.[25] Side chain assignments were made with (H)CC(CO)NH,[26] three-dimensional (3D) ^{15}N-separated NOESY-HSQC (200 ms mixing time),[27] 3D ^{13}C−^{15}N-separated HMQC-NOESY-HSQC [e.g., (H)CNH NOESY, 200 ms mixing time], 3D HCCH TOCSY,[28] 3D HCCH COSY,[29] and 3D ^{13}C-separated NOESY-HSQC (200 ms mixing time)[30] spectra. The protein was dried and resuspended in 100% D_2O (Cambridge Isotope Laboratories) twice, prior to HCCH COSY, HCCH TOCSY, and HCCH NOESY experiments. Spin systems for residues not visible in amide-resolved experiments were assigned via the 3D HCCH-TOCSY and 3D HCCH-COSY spectra and connectivity established with NOESY spectra. Spectra were processed with either NMRpipe[31] or Azara 2.7 (W. Boucher, Department of Biochemistry, University of Cambridge, Cambridge, U.K.) using maximum entropy reconstruction for the indirect dimensions in 3D experiments and analyzed with Sparky.[32] RDCs for NH vectors were measured in HSQC-IPAP experiments[33] via comparison of an unaligned sample of 0.2 mM LA45 versus an identical sample containing 10 mg/mL pf1 phage (Asla Biotech).

Structural Refinement. Peak lists from ^{13}C NOESY, ^{15}N NOESY, and HCN-NOESY (200 ms mixing time) spectra were analyzed with Aria2 for iterative NOE assignments;[34] 50 dihedral angle restraints were obtained from analysis of NH, H, Hα, CO, Cα, and Cβ chemical shifts using TALOS,[35] and 36 restraints to mimic the calcium coordination were added as described previously.[9] Hydrogen bond donors (six) were added on the basis of protection in H−D exchange experiments, and acceptors identified from initial structures. The six disulfide restraints were initially set as distance restraints and later set as covalent bonds. Manually assigned NOEs (112) involving the linker region were used as additional restraints. Rhombic and axial components of the alignment tensor (0.49 and 6.7, respectively) were estimated with the maximum likelihood approach,[36] and RDC values were included as susceptibility anisotropy (SANI) restraints with an error estimate of 0.4 Hz. Twenty structures from initial refinement with no NOE (>0.5 Å) or dihedral (>5°) violations were further refined using the distance geometry simulated annealing protocol in CNS 1.2,[37] with bona fide calcium restraints.[38] Root-mean-square deviations (rmsds) were calculated with Superpose 1.0.[39] NMR assignments and relevant data have been uploaded to BMRB (entry 16480), and coordinates have been deposited in the Protein Data Bank (PDB) as entry 2lgp. The figures were made using Pymol.[40]

Backbone Dynamics. Uniformly ^{15}N-labeled samples in the same NMR buffer were used to collect ^{15}N−{^{1}H} NOEs and ^{15}N T_1 and T_2 relaxation measurements at 33 °C. Relaxation measurement delays ranged from 5 ms to 3 s (T_1) and from 14 to 182 ms (T_2). Spectra with and without presaturation to determine the ^{15}N−{^{1}H} NOEs were recorded in an interleaved manner with a 6 s recycle delay. T_1 and T_2 relaxation measurements were fit to exponentials, and errors were obtained from the uncertainty of the fit and from occasional duplicate points yielding similar uncertainties. The ^{15}N−{^{1}H} NOEs were calculated from the ratio of peak heights in duplicate, and errors are the standard deviations. For H−D exchange experiments, 0.4 mM ^{15}N-labeled samples in the same NMR buffer were dried and resuspended in either 10% D_2O or 100% D_2O, and a series of ^{1}H−^{15}N HSQC spectra were recorded from 15 min to 2 h at 25 °C. Data were processed with NMRpipe[31] and analyzed with Sparky.[32] Tensor 2.0 was used for model free fitting of relaxation data with 100 cycles of Monte Carlo simulations for error analysis.[41] Theoretical correlation times based on atomic coordinates were calculated with HYDRONMR.[42] An atomic element radius (5.2 Å) was found to predict the observed value for LA5 (predicted value of 3.66 ns vs measured value of 3.68 ns) and was used for subsequent calculations on all constructs.

Ligand Titrations. Dried ^{15}N-labeled LA modules (40 nmol) were resuspended in 400 μL of either 0.5 mM ubiquitin or Ub-RAPD3. The samples were mixed in ratios to yield

several concentrations of RAPD3 between 0 and 500 μM, and each was monitored by $^{1}H-^{15}N$ HSQC. Ub-ApoE(130−149) titrations were conducted in the same manner but with higher concentrations of titrant (>1 mM). The chemical shifts were analyzed as a function of titrant concentration in both dimensions, with ^{15}N shifts scaled down by the $^{1}H/^{15}N$ gyromagnetic ratio (9.8). K_D values and errors were calculated as described previously.[21,43]

RESULTS

Refolding of LA4. The LDLR LAs each contain six cysteines that form three disulfide bonds, and it was therefore necessary to produce them in *Escherichia coli* in an unfolded state and refold them under disulfide exchange conditions.[4] Unlike LA5 and LA3, LA4 did not efficiently refold to one disulfide-bonded isomer, in agreement with previous observations.[13] LA4 was isolated as a single peak by analytical HPLC with the expected mass, but the $^{1}H-^{15}N$ HSQC spectrum showed more than the expected number of cross-peaks (56 and 41), indicating heterogeneity. Reverse phase HPLC purification in ammonium acetate at pH 5.5 with 5 mM $CaCl_2$ resolved three species of LA4 (Figure 2A). Because the mass of each

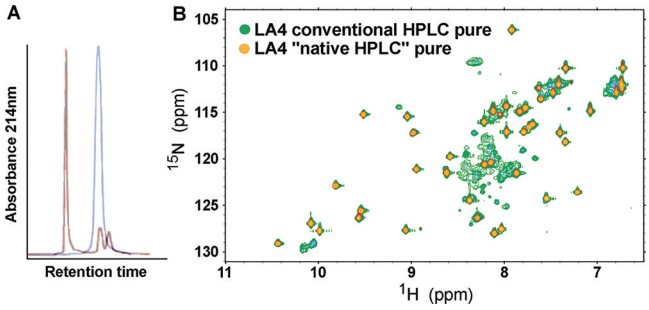

Figure 2. (A) Overlay of the analytical HPLC traces of purified LA4 in either 0.1% TFA (blue) or 10 mM NH_4OAc (pH 5.5) with 5 mM $CaCl_2$ (red). (B) Overlay of the HSQC spectra of LA4 after conventional HPLC purification (green) or after HPLC purification under native (calcium bound) conditions (gold).

species was that expected for LA4 (measured value of 5118.7 ± 3 Da vs theoretical value of 5120.9 Da), it was likely that distinct disulfide bond isomers were present. Only the earliest eluting, major peak had a dispersed HSQC spectrum with even line shapes, reflective of a well-folded protein (Figure 2B). Refolding of the tandem constructs of LA45 and LA345 resulted in similar amounts of misfolded species, suggesting that contact with neighboring modules did not assist in the proper refolding of LA4.

Calcium Binding. The calcium affinity of each module was measured by ITC. The binding isotherms of LA3 and LA5 showed strong binding to a single calcium ion with thermodynamic properties similar to those described in previous reports (Figure 3A,C).[5] However, LA4 reproducibly yielded a hyperbolic curve corresponding to a significantly weaker calcium affinity [K_D = 163 μM (Figure 3B and Table 1)], weaker than that of any module tested to date.[5,15,44,45] This result was consistent with the observation that HSQC spectra of LA4 showed the best dispersion and line widths at calcium concentrations of ≥5 mM. Titrations with LA4 were repeated at pH 5.2, and calcium affinity was even weaker, with a K_D of 546 μM (Figure 3D).

To test whether calcium binding of LA4 would be different when it was connected to LA5, as it is in the full-length LDLR, we also tested calcium binding to LA45. The calcium binding isotherm of LA45 showed strong binding to only a single calcium ion (Figure 3E). Thermodynamic parameters from fitting to a two-site model were consistent with one calcium ion binding to LA5 with high affinity, and the second binding with weak affinity to LA4. Because of the weak binding isotherm, the thermodynamic parameters for the second calcium binding event could not be determined with a high degree of certainty.

Structure of LDLR LA45. The structure of LA45, refolded and purified under native HPLC conditions, was determined by NMR at pH 7.4. HSQC spectra of LA45 compared to those of each isolated module showed only weak perturbations resulting from linkage (Figure 5A and Figure S1 of the Supporting Information). While some of these chemical shift differences were not proximal to the linker, the result suggested that each module was structured independently. No changes in peak width or position were observed over a range of concentrations from 0.1 to 1.0 mM, indicating no significant self-association occurred under these experimental conditions. 3D ^{15}N-separated NOESY-HSQC, 3D ^{13}C-separated NOESY-HSQC, and 3D $^{13}C-^{15}N$-separated HMQC-NOESY-HSQC [(H)CNH NOESY] spectra were analyzed with Ambiguous Restraint for Iterative Assignment (ARIA2), yielding a total of 2453 NOE-based distance restraints (1850 unambiguous and 603 ambiguous). Amide cross-peaks for residues 171−174 were not observed, and only weak NOEs were observed for this region in the 3D ^{13}C-separated NOESY-HSQC spectrum. Residual dipolar couplings (RDCs) (55) were obtained from the difference in dipolar coupling between aligned and unaligned samples from HSQC-IPAP experiments. Additional restraints for final structural calculations included 50 chemical shift-derived dihedral restraints (TALOS), 12 calcium binding restraints, six hydrogen bonds, and six disulfide bonds (see Methods and Table 2).

The superposition of the 20 lowest-energy structures on either LA4 or LA5 (Figure 4) showed the structure of each module was well resolved, with backbone rmsds of 0.38 Å for LA4 and 0.28 Å for LA5 (Table 2). No NOEs were observed between the two domains; however, NOEs were observed between linker residues R164−Y167 and LA4. Although this constrained the N-terminal half of the 12-residue linker, the C-terminal part of the linker remained ill-defined, resulting in diverse interdomain orientations within the ensemble. RDCs fit to each LA45 structure within the ensemble using PALES[46] gave a correlation between experimental and theoretical values of >0.9, indicating that although highly variable, each relative domain orientation was consistent with the RDC data.

Backbone Dynamics. NMR dynamics measurements were used to investigate whether intrinsic dynamics of these modules changes in the context of the linked module pair. H−D exchange experiments with LA45 conducted at pH 7.4 identified several amides in LA5 (E180, F181, C183, S185, I189, W193, R194, C195, D196, D200, C201, S205, D206, and E207) that were protected for hours, whereas all amides in LA4 were exchanged within minutes. R_1 and R_2 relaxation rates and $^{15}N-\{^{1}H\}$ NOEs were measured for LA4, LA5, and LA45 under identical conditions (Figure S2 of the Supporting Information). R_2 relaxation rates for LA4 were higher than for LA5 (averages of 7.5 and 6.0 s^{-1}, respectively), suggesting the presence of chemical exchange within LA4. Order parameters (S^2) from model free fitting also show LA4 as

dx.doi.org/10.1021/bi2014486 | *Biochemistry* 2011, 50, 11001−11008

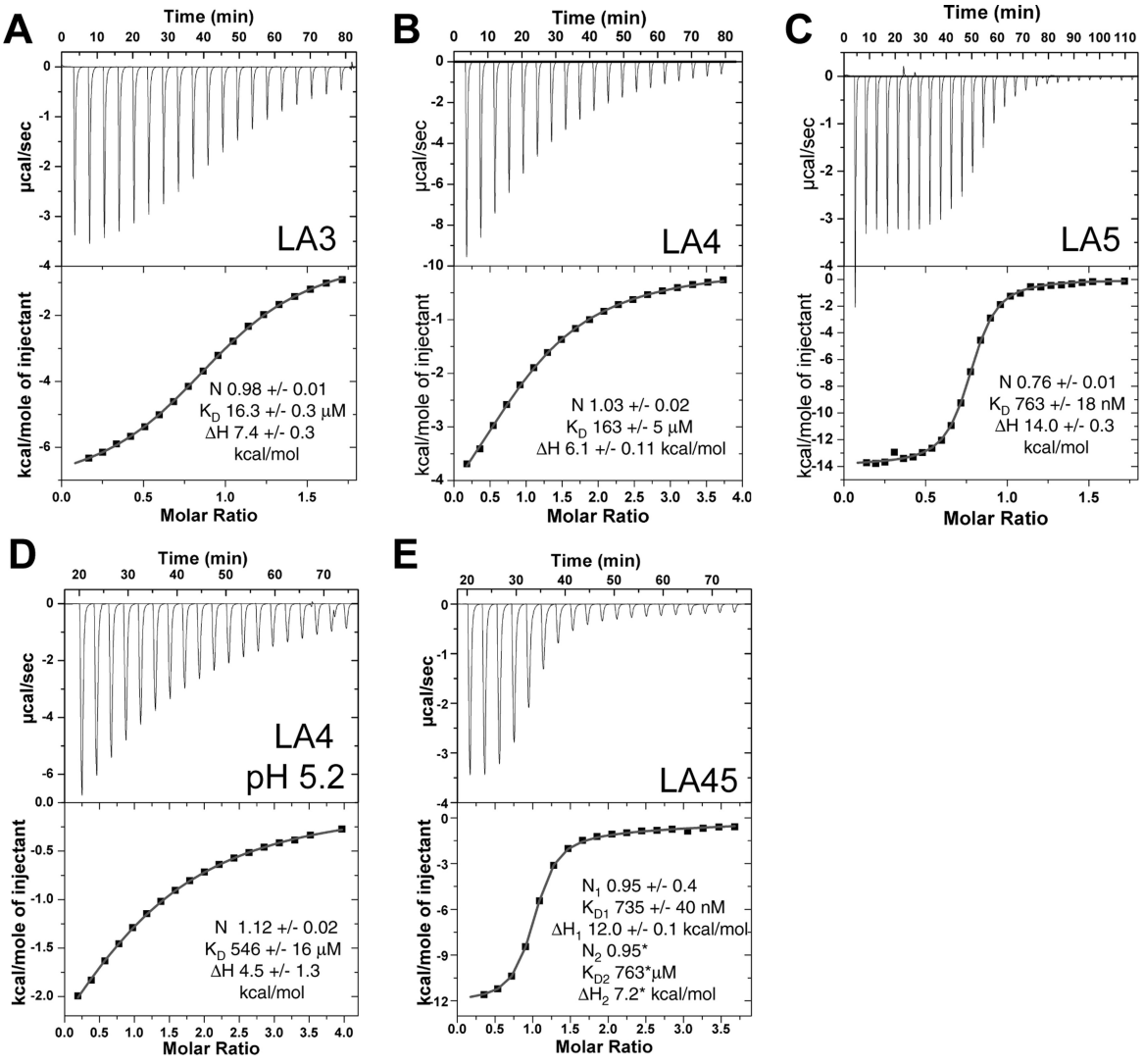

Figure 3. Calcium binding isotherms for (A) LA3, (B) LA4, (C) LA5, and (D) LA4 at pH 5.2 and (E) LA45 at pH 7.4.

Table 1. Binding Affinities of Calcium and Ligands for LDLR Fragment Pairs

ligand	LA	K_D (μM)
calcium[a]	LA3 alone	16 ± 0.25
	LA4 alone	173 ± 14
	LA5 alone	0.76 ± 0.05
	LA4 (in LA45)	763 ± ND[c]
	LA5 (in LA45)	0.74 ± 0.04
	LA4 (pH 5.2)	546 ± 16
RAPD[32]	LA4 alone	49 ± 3
	LA5 alone	670 ± 26
ApoE(130−149)[b]	LA4 alone	1090 ± 90
	LA4 in LA45	405 ± 41
	LA5 alone	3880 ± 290
	LA5 in LA45	730 ± 160

[a]From isothermal titration calorimetry experiments. [b]From NMR titration experiments. [c]Uncertainty very high because of the weak binding isotherm.

being overall less ordered than LA5 (Figure 5B). Estimates of the rotational correlation time from R_2/R_1 indicate that the module pair undergoes a degree of correlated tumbling (4.4 ± 0.8, 3.7 ± 0.6, and 7.6 ± 0.9 ns for LA4, LA5, and LA45, respectively). Comparison of the order parameters of the isolated modules with that of the tandem LA45 revealed that regions of the calcium binding site in both LA4 (residues 145−151) and LA5 (residues 196−202) are more ordered in the module pair (Figure 5B). Although most linker amides showed significant exchange broadening making it impossible to obtain relaxation data for this region, the $^{15}N-\{^1H\}$ NOEs for residues 166−170 in the N-terminal half of the linker were much higher than in LA4 alone, indicating a significant degree of ordering of the first part of the linker in the domain pair (Figure S2 of the Supporting Information). The $^{15}N-\{^1H\}$ NOEs decrease from the N-terminal to the C-terminal residues of the linker, and the C-terminal half appears to retain a high degree of flexibility.

Specific dynamic changes arising from interdomain connection were similar to the observed chemical shift perturbations arising from linkage. In the case of LA5, several amides showing large chemical shift perturbations upon linkage (H182, E187, G198, and D200) also show significant differences in S^2 parameters and $^{15}N-\{^1H\}$ NOEs (Figure 5B and Figure S2 of the Supporting Information).

RAPD3 and ApoE(130−149) Binding. Ligand titrations were used to characterize binding of RAPD3 to each single

dx.doi.org/10.1021/bi2014486 | *Biochemistry* 2011, 50, 11001−11008

Table 2. NMR Structural Statistics

no. of NMR constraints	
distance constraints	2453
intraresidue	389
sequential ($\|i - j\| = 1$)	499
medium-range ($\|i - j\| < 4$)	424
long-range ($\|i - j\| > 5$)	538
ambiguous	603
hydrogen bonds	6
dihedral angle restraints	50
residual dipolar coupling restraints	55
structural statistics (20 structures)	
rmsd from idealized covalent geometry	
bond lengths (Å)	0.0016 ± 0.00013
bond angles (deg)	0.3290 ± 0.02219
impropers (deg)	0.2044 ± 0.02155
rmsd from distance constraints (Å)	0.0414 ± 0.00359
rmsd from dihedral angle constraints (deg)	0.6222 ± 0.70447
coordinate precision	
average pairwise rmsd (residues 127−163) (Å) (LA4)	
all backbone atoms	0.38 ± 0.11
all heavy atoms	0.58 ± 0.13
average pairwise rmsd (residues 176−210) (Å) (LA5)	
all backbone atoms	0.28 ± 0.13
all heavy atoms	0.51 ± 0.15
Ramachandran plot statistics (residues 127−163 and 176−210) (%)	
most favored regions	64.4
additionally allowed regions	30.7
generously allowed regions	4.6
disallowed regions	0.2

module and to LA45 using Ub-fused RAPD3 and Ub alone as the negative control (see Methods). HSQC spectra showed specific chemical shift perturbations within LA4 and LA5 upon binding of Ub-RAPD3 (Figure S3 of the Supporting Information). The strongest shifts in LA45 (L143, D149, E158, H190, S192, G198, and side chain ε1 of W144 and W193) were consistent with those seen in titrations with the individual modules. The affinities of LA4 and LA5 for Ub-RAPD3 calculated from these titrations yielded K_D values of 49 and 670 μM, respectively (Table 1). LA45 was fully bound even at a 1/1 ratio with Ub-RAPD3, indicative of significantly tighter binding, as expected for the interaction of the two-module pair.[47] Furthermore, LA45 remained bound to Ub-RAPD3 through size exclusion chromatography in a calcium-dependent manner, as seen previously with the LA34·RAPD3 complex.[6]

NMR titrations of Ub-ApoE(130−149) with each isolated module and the module pair were also performed. Perturbations for binding of Ub-ApoE(130−149) to the isolated LA4 and LA5 were essentially the same as those observed upon Ub-RAPD3 binding (Figure S4 of the Supporting Information). The perturbations were also the same upon titration of the linked module pair (Figure 5C); however, the binding affinity of both LA4 and LA5 was dramatically enhanced in the double-module construct (405 μM vs 1090 μM for LA4 and 730 μM vs 3880 μM for LA5) (Figure 6 and Table 1). Notably, the two modules in the LA45 pair have a very distinct K_D, well outside of the error, suggesting that each module binds a separate molecule of Ub-ApoE(130−149).

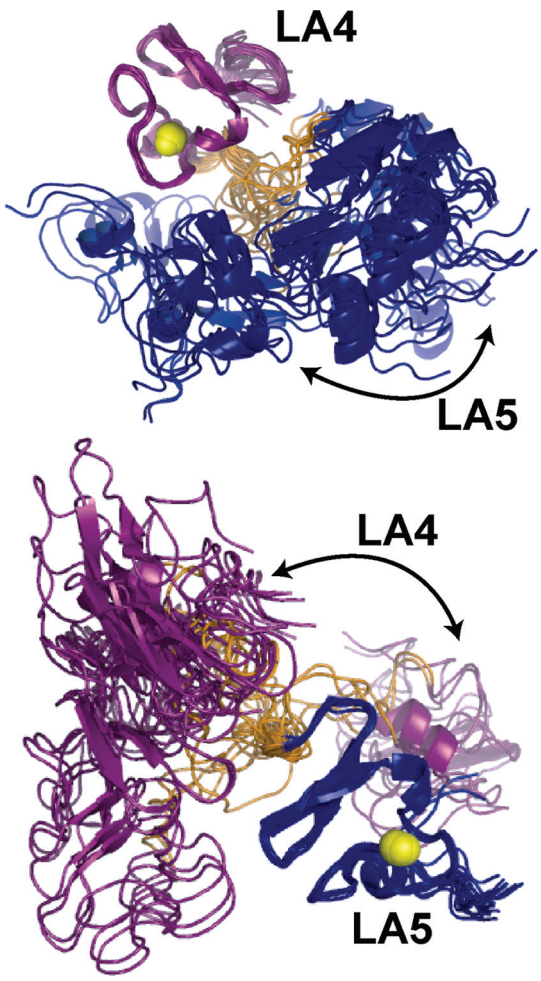

Figure 4. Superposition of the 20 lowest-energy structures of LA45 with LA4 (purple), linker (orange), LA5 (blue), and calcium ions (yellow spheres). Structures are aligned with either residues 127−163 of LA4 (top) or residues 176−210 of LA5 (bottom).

DISCUSSION

Structural Similarity of LA Modules. The structures of each individual module in LA45 are similar to the previously determined structures. The all atom rmsd of LA4 determined here compared to LA4 in the LA34·RAPD3 complex was 1.74 Å,[6] and that for LA5 compared with the crystal structure of LA5 was 1.85 Å.[4] Larger structural differences were seen when comparisons were made to the endosomal LDLR structure (Figure 7).[2] The structural differences in the loop containing H190 (LA5) are likely attributed to the interaction of these regions with the β-propeller domain.[2] This same region undergoes one of the largest chemical shift perturbations upon ApoE(130−149) binding, strengthening the notion that they are involved in the ApoE−LDLR interaction.[21,48]

Linker between LA4 and LA5. Across species, evolution has conserved the length (12−14 residues) of the linker between LA4 and LA5 without conservation of any specific residues, which is typically seen for flexible linkers (Figure S5 of the Supporting Information). Truncation of this linker significantly alters the interaction with LDL particles, hinting that it may be required for the two modules to access distant epitopes on ligands such as multiple copies of ApoE on a lipoprotein surface.[17] The ApoE-binding pair of modules, 5 and 6, from the very low-density lipoprotein receptor (VLDLR),

dx.doi.org/10.1021/bi2014486 | Biochemistry 2011, 50, 11001−11008

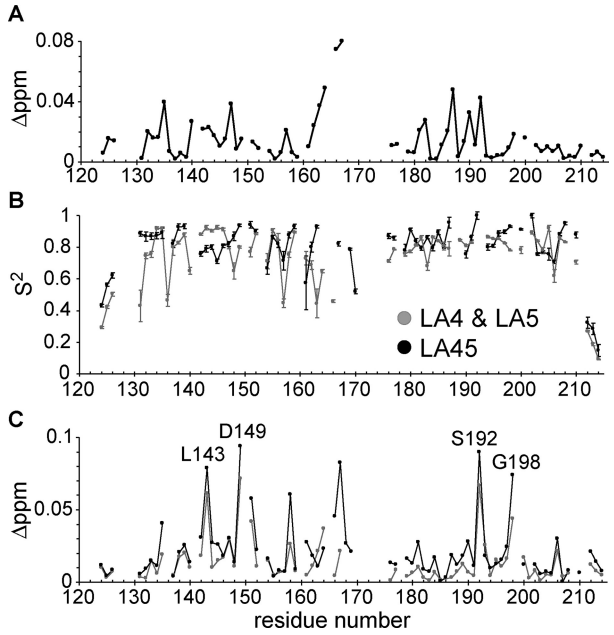

Figure 5. (A) Chemical shift differences (^{1}H and ^{15}N; see Methods) between LA45 and each isolated module. (B) Order parameters (S^2) obtained from model free fitting of relaxation data for LA45 (black) and isolated LA4 and LA5 (gray) (R_1, R_2, and ^{15}N–{^{1}H} NOE are shown in Figure S2 of the Supporting Information). (C) Chemical shift perturbations of LA45 (black) and both isolated modules (gray) upon binding ApoE(130–149). Residues showing the largest changes are labeled.

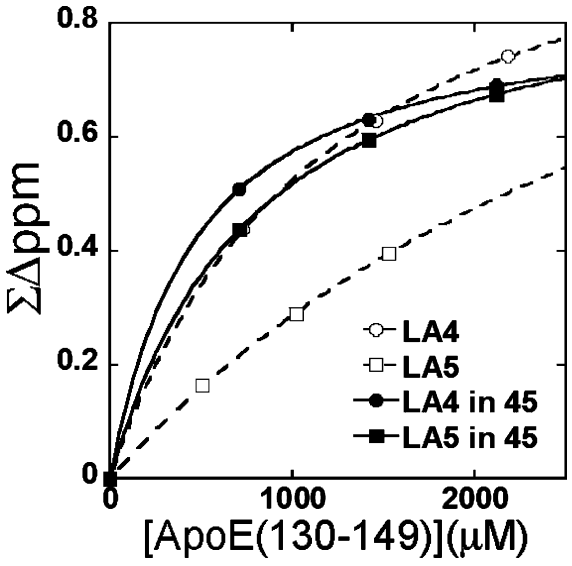

Figure 6. Titration fits of Ub-ApoE(130–149) binding isolated LA4 (○), isolated LA5 (□), LA4 in LA45 (●), and LA5 in LA45 (■). Plots are sum total of the magnitude of the perturbations (in parts per million) plotted vs ApoE(130–149) concentration.

also have a longer linker (nine residues),[52] but the sequence of this linker is conserved. It will be interesting to see whether LA56 in VLDLR shows similar dynamic properties.

Interdomain Cross Talk. It is not uncommon that weak interdomain interactions govern relative orientations even in the absence of any observable interdomain NOEs.[53,54] LA12 showed a preferred perpendicular orientation despite the absence of NOEs between the two domains, and the larger τ_c of LA5 (2.8 ns) in LA56 (4.6 ns) was attributed to spatial occlusion.[14,55] The τ_c of LA5 in LA45 was also considerably longer (7.6 ns vs 3.7 ns) possibly because of similar spatial occlusion, which is remarkable because the linker for LA45 is 3 times longer than that between LA5 and LA6. HYDRONMR calculations predict a τ_c of 9.2 ± 0.9 ns for the LA45 ensemble, still larger than the observed value of 7.6 ns, again consistent with some but not complete restriction of the interdomain orientation. In an attempt to resolve the LA4–LA5 relative domain orientation ambiguity, we collected RDCs on the LA4–LA5 domain pair. Although the possible orientations are somewhat confined, mostly because of the restrains to the N-terminal half of the linker, the RDC restraints were consistent with a range of domain orientations. Together with the absence of interdomain NOEs, this result suggests that LA45 does not form rigid interdomain contacts, with only transient interactions limiting its domain motions.

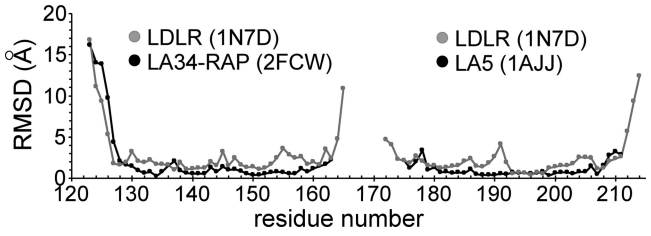

Figure 7. Root-mean-square deviations (backbone only) of the structure of LA45 determined here by NMR at physiological pH compared to the structure of LA45 from the crystal structure of the LDLR at endosomal pH from PDB entry 1ND7 (gray). LA4 from PDB entry 2fcw and LA5 from PDB entry 1ajj (black).

Functional Consequences for Ligand Binding. Both NMR and cryo-EM studies have shown that many LA modules act as isolated units, and it has been suggested that this provides flexibility to bind a diversity of ligands.[12–15,55] Despite the long, relatively flexible linker connecting them, the LA45 modules appear to be influenced by the presence of their neighbors. Weak intermolecular effects had been previously observed for module pairs, [55] but consequences of this type of cross talk have not yet been examined. Here we present evidence that ligand affinity correlates with the effects of the observed intermodule cross talk.

Our previous functional studies showed that LA4 primarily interacts with the canonical ApoE receptor binding region [ApoE(130–149)].[21] The backbone dynamics of LA4 presented here show changes at residues 142–152, residues critical for ApoE binding, when linked to LA5 (Figure 5B). It is likely that these effects are at least partly responsible for the observed enhancement of ApoE(130–149) binding by the module pair as compared to that with isolated LA4. The same titrations showed that linkage also leads to changes at the LA5 ligand binding site as well, although ApoE(130–149) may not represent the relevant binding partner as LA5 is thought to bind a distinct epitope involving ApoE residues 186–193.[21] Interestingly, the modules in both LA12 and LA56 undergo minor chemical shift perturbations when linked,[13,15] and weak interdomain cross talk may be occurring in these module pairs, as well.

Functional Consequences of the Weak Calcium Affinity of LA4. LA4 exhibited the lowest affinity for calcium compared to all other members of this class of protein modules.[45] Calcium binding to LA4 has only previously been tested using a four-repeat construct, LA3456,[18] in which the

weak binding isotherm of this particular module is likely to be miniscule, just as we observed in LA45. Because LA modules depend on calcium coordination for their native fold,[11] the weak calcium affinity may be the reason this repeat refolds poorly[13] and may be related to the higher backbone dynamics in LA4 compared to those in LA5 and other repeats. However, LA1 and LA2, which have similar affinities for calcium, have very different backbone dynamics.[8,13,14] Another possibility is that the octahedral geometry for the calcium binding site in LA4 is distorted, possibly by P150. A Pro at this position is rare among LA modules in the LDLR family. In the case of LA5, G198 may offset the distortion imposed by P199 (at the equivalent position of P150) to allow for a more favorable calcium binding geometry.

The weak calcium affinity of LA4 may have functional relevance regarding ligand release. Calcium ion occupancy is necessary for LDL modules to bind ligands.[11] LA4 would be more than 90% calcium-bound at serum calcium ion levels of ~2 mM;[49] however, at an endosomal calcium ion concentration of 10 μM,[50] it would be only 5% bound. The acidic environment in the endosome further reduces the affinity, resulting in a calcium ion occupancy for LA4 near zero, which would cause or at least contribute to ligand release. These results are consistent with the recent model in which both low pH and low Ca^{2+} concentration trigger LDL release[3] but indicate that LA4 rather than LA5, as suggested previously,[51] is the critical module that triggers ligand release in the endosome.

■ ASSOCIATED CONTENT

Ⓢ Supporting Information

Additional figures and data. This material is available free of charge via the Internet at http://pubs.acs.org.

Accession Codes

Atomic coordinates of the 20 lowest-energy structures of LA45 have been deposited in the Protein Data Bank as entry 2lgp.

■ AUTHOR INFORMATION

Corresponding Author

*E-mail: ekomives@ucsd.edu. Phone: (858) 534-3058.

Funding

This work was supported by National Institutes of Health Grant RO1 AG025343. M.G. was supported by Heme and Blood Proteins Training Grant T32-DK007233.

■ ACKNOWLEDGMENTS

We thank Joseph Noel at the Salk Institute for the pHis8 vector and Tracy M. Handel and Peter Domaille for help with the NMR experiments.

■ ABBREVIATIONS

GST, glutathione *S*-transferase; RAP, receptor-associated protein; CR, complement repeat; LA, ligand binding repeat; NMR, nuclear magnetic resonance; MALDI-TOF, matrix-assisted laser desorption ionization time-of-flight; LDLR, low-density lipoprotein receptor; HPLC, high-performance liquid chromatography; HSQC, heteronuclear single-quantum coherence; ITC, isothermal titration calorimetry; NOE, nuclear Overhauser effect; τ_c, rotational correlation time.

■ REFERENCES

(1) Blacklow, S. C. (2007) Versatility in ligand recognition by LDL receptor family proteins: Advances and frontiers. *Curr. Opin. Struct. Biol. 17*, 419−426.

(2) Rudenko, G., Henry, L., Henderson, K., Ichtchenko, K., Brown, M. S., Goldstein, J. L., and Deisenhofer, J. (2002) Structure of the LDL receptor extracellular domain at endosomal pH. *Science 298*, 2353−2358.

(3) Zhao, Z., and Michaely, P. (2009) The Role of Calcium in Lipoprotein Release by the Low-Density Lipoprotein Receptor. *Biochemistry 48*, 7313−7324.

(4) Fass, D., Blacklow, S., Kim, P. S., and Berger, J. M. (1997) Molecular basis of familial hypercholesterolaemia from structure of LDL receptor module. *Nature 388*, 691−693.

(5) Simonovic, M., Dolmer, K., Huang, W., Strickland, D. K., Volz, K., and Gettins, P. G. W. (2001) Calcuim coordination and pH dependence of the calcium affinity of ligand-binding repeat CR7 from the LRP. Comparision with related domains from the LRP and the LDL receptor. *Biochemistry 40*, 15127−15134.

(6) Fisher, C., Beglova, N., and Blacklow, S. C. (2006) Structure of an LDLR-RAP complex reveals a general mode for ligand recognition by lipoprotein receptors. *Mol. Cell 22*, 277−283.

(7) Daly, N. L., Scanlon, M. J., Djordjevic, J. T., Kroon, P. A., and Smith, R. (1995) Three-dimernsional structure of a cysteine-rich repeat from the low-density lipoprotein receptor. *Proc. Natl. Acad. Sci. U.S.A. 92*, 6334−6338.

(8) Daly, N. L., Djordjevic, J. T., Kroon, P. A., and Smith, R. (1995) Three-dimensional structure of the second cysteine-rich repeat from the human low-density lipoprotein receptor. *Biochemistry 34*, 14474−14481.

(9) North, C. L., and Blacklow, S. C. (2000) Solution structure of the sixth LDL-A module of the LDL receptor. *Biochem. J. 39*, 2564−2571.

(10) Guo, Y., Yu, X., Rihani, K., Wang, Q. Y., and Rong, L. (2004) The role of a conserved acidic residue in calcium-dependent protein folding for a low density lipoprotein (LDL)-A module: Implications in structure and function for the LDL receptor superfamily. *J. Biol. Chem. 279*, 16629−16637.

(11) Blacklow, S. C., and Kim, P. S. (1996) Protein folding and calcium binding defects arising from familial hypercholesterolemia mutations of the LDL receptor. *Nat. Struct. Biol. 3*, 758−762.

(12) Jeon, H., and Shipley, G. G. (2000) Vesicle-reconstituted low density lipoprotein receptor. Visualization by cryoelectron microscopy. *J. Biol. Chem. 275*, 30458−30464.

(13) Bieri, S., Atkins, A. R., Lee, H. T., Winzor, D. J., Smith, R., and Kroon, P. A. (1998) Folding, Calcium Binding, and Structural Characterization of a Concatemer of the First and Second Ligand-Binding Modules of the Low-Density Lipoprotein Receptor. *Biochemistry 37*, 10994−11002.

(14) Kurniawan, N. D., Atkins, A. R., Bieri, S., Brown, C. J., Brereton, I. M., Kroon, P. A., and Smith, R. (2000) NMR structure of a concatemer of the first and second ligand-binding modules of the human low-density lipoprotein receptor. *Protein Sci. 9*, 1282−1293.

(15) North, C. L., and Blacklow, S. C. (1999) Structural independence of ligand-binding modules five and six of the LDL receptor. *Biochem. J. 38*, 3926−3935.

(16) Esser, V., Limbird, L. E., Brown, M. S., Goldstein, J. L., and Russell, D. W. (1988) Mutational analysis of the ligand binding domain of the low density lipoprotein receptor. *J. Biol. Chem. 263*, 13282−13290.

(17) Russell, D. W., Brown, M. S., and Goldstein, J. L. (1989) Different combinations of cysteine-rich repeats mediate binding of low density lipoprotein receptor to two different proteins. *J. Biol. Chem. 264*, 21682−21688.

(18) Fisher, C., Abdul-Aziz, D., and Blacklow, S. C. (2004) A two-module region of the low-density lipoprotein receptor sufficient for formation of complexes with apolipoprotein E ligands. *Biochem. J. 43*, 1037−1044.

(19) Yamamoto, T., and Ryan, R. O. (2009) Domain swapping reveals that low density lipoprotein (LDL) type A repeat order affects ligand binding to the LDL receptor. *J. Biol. Chem. 284*, 13396−133400.
(20) Ren, G., Rudenko, G., Ludtke, S. J., Deisenhofer, J., Chiu, W., and Pownall, H. J. (2010) Model of human low-density lipoprotein and bound receptor based on cryoEM. *Proc. Natl. Acad. Sci. U.S.A. 107*, 1059−1064.
(21) Guttman, M., Prieto, J. H., Croy, J. E., and Komives, E. A. (2010) Decoding of lipoprotein−receptor interactions: Properties of ligand binding modules governing interactions with ApoE. *Biochemistry 49*, 1207−1216.
(22) Jez, J. M., Ferrer, J. L., Bowman, M. E., Dixon, R. A., and Noel, J. P. (2000) Dissection of Malonyl-Coenzyme A Decarboxylation from Polyketide Formation in the Reaction Mechanism of a Plant Polyketide Synthase. *Biochemistry 39*, 890−902.
(23) Grzesiek, S., and Bax, A. (1992) An Efficient Experiment for Sequential Backbone Assignment of Medium-Sized Isotopically Enriched Proteins. *J. Magn. Reson. 99*, 201−207.
(24) Grzesiek, S., and Bax, A. (1992) Correlating backbone amide and side chain resonances in larger proteins by multiple relayed triple resonance NMR. *J. Am. Chem. Soc. 114*, 6291−6293.
(25) Kay, L. E., Ikura, M., Tschudin, R., and Bax, A. (1990) Three-dimensional triple-resonance NMR spectroscopy of isotopically enriched proteins. *J. Magn. Reson. 89*, 496−514.
(26) Clowes, R. T., Boucher, W., Hardman, C. H., Domaille, P. J., and Laue, E. D. (1993) A 4D HCC(CO)NNH experiment for the correlation of aliphatic side-chain and backbone resonances in $^{13}C/^{15}N$-labelled proteins. *J. Biomol. NMR 3*, 349−354.
(27) Talluri, S., and Wagner, G. (1996) An Optimized 3D NOESY-HSQC. *J. Magn. Reson. 112*, 200−205.
(28) Bax, A., Clore, G. M., and Gronenborn, A. M. (1990) Proton-proton correlation via isotropic mixing of carbon-13 magnetization, a new three-dimensional approach for assigning proton and carbon-13 spectra of carbon-13-enriched proteins. *J. Magn. Reson. 88*, 425−431.
(29) Ikura, M., Kay, L. E., and Bax, A. (1991) Improved three-dimensional ^{1}H-^{13}C-^{1}H spectroscopy of a ^{13}C-labeled protein using constant-time evolution. *J. Biomol. NMR 1*, 299−304.
(30) Zuiderweg, E. R. P., McIntosh, L. P., Dahlquist, F. W., and Fesik, S. W. (1990) Three-dimensional carbon-13-resolved proton NOE spectroscopy of uniformly carbon-13-labeled proteins for the NMR assignment and structure determination of larger molecules. *J. Magn. Reson. 86*, 210−216.
(31) Delaglio, F., Grzesiek, S., Vuister, G., Zhu, G., Pfeifer, J., and Bax, A. (1995) NMRPipe: A multidimensional spectral processing system based on UNIX pipes. *J. Biomol. NMR 6*, 277−293.
(32) Goddard, T. D., and Kneller, D. G. (2007) *SPARKY 3*, University of California, San Francisco.
(33) Cordier, F., Dingley, A. J., and Grzesiek, S. (1999) A doublet-separated sensitivity-enhanced HSQC for the determination of scalar and dipolar one-bond J-couplings. *J. Biomol. NMR 13*, 175−180.
(34) Rieping, W., Habeck, M., Bardiaux, B., Bernard, A., Malliavin, T. E., and Nilges, M. (2007) ARIA2: Automated NOE assignment and data integration in NMR structure calculation. *Bioinformatics 23*, 381−382.
(35) Cornilescu, G., Delaglio, F., and Bax, A. (1999) Protein backbone angle restraints from searching a database for chemical shift and sequence homology. *J. Biomol. NMR 13*, 298−302.
(36) Warren, J. J., and Moore, P. B. (2001) A Maximum Likelihood Method for Determining DaPQ and R for Sets of Dipolar Coupling Data. *J. Magn. Reson. 149*, 271−275.
(37) Brunger, A. T. (2007) Version 1.2 of the Crystallography and NMR System. *Nat. Protoc. 2*, 2728−2733.
(38) Jensen, G. A., Andersen, O. M., Bonvin, A. M., Bjerrum-Bohr, I., Etzerodt, M., Thøgersen, H. C., O'Shea, C., Poulsen, F. M., and Kragelund, B. B. (2006) Binding site structure of one LRP-RAP complex: Implications for a common ligand-receptor binding motif. *J. Mol. Biol. 362*, 700−716.
(39) Maiti, R., Van Domselaar, G. H., Zhang, H., and Wishart, D. S. (2004) SuperPose: A simple server for sophisticated structural superposition. *Nucleic Acids Res. 32*, 590−594.
(40) DeLano, W. L. (2002) *The PyMOL Molecular Graphics System*, DeLano Scientific, San Carlos, CA.
(41) Cordier, F., Caffrey, M., Brutscher, B., Cusanovich, M. A., Marion, D., and Blackledge, M. (1998) Solution structure, rotational diffusion anisotropy and local backbone dynamics of *Rhodobacter capsulatus* cytochrome c_2. *J. Mol. Biol. 281*, 341−361.
(42) García de la Torre, J., Huertas, M. L., and Carrasco, B. (2000) HYDRONMR: Prediction of NMR relaxation of globular proteins from atomic-level structures and hydrodynamic calculations. *J. Magn. Reson. 147*, 138−146.
(43) Hoffman, R. M. B., Li, M. X., and Sykes, B. D. (2005) The Binding of W7, an Inhibitor of Striated Muscle Contraction, to Cardiac Troponin C. *Biochemistry 44*, 15750−15759.
(44) Andersen, O. M., Vorum, H., Honoré, B., and Thøgersen, H. C. (2003) Ca^{2+} binding to complement-type repeat domains 5 and 6 from the low-density lipoprotein receptor-related protein. *BMC Biochem. 4* (7), 1−7.
(45) Rudenko, G., and Deisenhofer, J. (2003) The low-density lipoprotein receptor: Ligands, debates and lore. *Curr. Opin. Struct. Biol. 13*, 683−689.
(46) Zweckstetter, M. (2008) NMR: Prediction of molecular alignment from structure using the PALES software. *Nat. Protoc. 3*, 679−690.
(47) Andersen, O. M., Schwarz, F. P., Eisenstein, E., Jacobsen, C., Moestrup, S. K., Etzerodt, M., and Thøgersen, H. C. (2001) Dominant thermodynamic role of the third independent receptor binding site in the receptor-associated protein RAP. *Biochem. J. 40*, 15408−15417.
(48) Abdul-Aziz, D., Fisher, C., Beglova, N., and Blacklow, S. C. (2005) Folding and binding integrity of variants of a prototype ligand-binding module from the LDL receptor possessing multiple alanine substitutions. *Biochem. J. 44*, 5075−5085.
(49) Marshall, W. J. (1995) in *Clinical Chemistry*, Mosby, London.
(50) Gerasimenko, J. V., Tepikin, A. V., Petersen, O. H., and Gerasimenko, O. V. (1998) Calcium uptake via endocytosis with rapid release from acidifying endosomes. *Curr. Biol. 8*, 1335−1338.
(51) Arias-Moreno, X., Velazquez-Campoy, A., Rodríguez, J. C., Pocovı, M., and Sancho, J. (2008) Mechanism of low density lipoprotein (LDL) release in the endosome: Implications of the stability and Ca^{2+} affinity of the fifth binding module of the LDL receptor. *J. Biol. Chem. 283*, 22670−22679.
(52) Ruiz, J., Kouiavskaia, D., Migliorini, M., Robinson, S., Saenko, E. L., Gorlatova, N., Li, D., Lawrence, D., Hyman, B. T., Weisgraber, K. H., and Strickland, D. K. (2005) The apoE isoform binding properties of the VLDL receptor reveal marked differences from LRP and the LDL receptor. *J. Lipid Res. 46*, 1721−1731.
(53) Murphy, J. M., Hansen, F. D., Wiesner, S., Muhandiram, R. D., Borg, M., Smith, M. J., Sicheri, F., Kay, L. E., Forman-Kay, J. D., and Pawson, T. (2009) Structural Studies of FF Domains of the Transcription Factor CA150 Provide Insights into the Organization of FF Domain Tandem Arrays. *J. Mol. Biol. 393*, 409−424.
(54) Spitzafden, C., Grant, R. P., Mardon, H. J., and Campbell, I. D. (1997) Module-Module Interactions in the Cell Binding Region of Fibronectin: Stability, Flexibility and Specificity. *J. Mol. Biol. 265*, 565−579.
(55) Beglova, N., North, C. L., and Blacklow, S. C. (2001) Backbone dynamics of a module pair from the ligand-binding domain of the LDL receptor. *Biochemistry 40*, 2808−2815.